LIGHT-WEIGHT CONTAINMENT FOR HIGH ENERGY, ROTATING MACHINES

By:

J.L. Strubhar
R.C. Thompson
T.T. Pak
J.J. Zierer
J.H. Beno
R.J. Hayes

Eleventh EML Technology Symposium, Saint-Louis, France, May 14-17, 2002

Attached paper is the final version as submitted to the conference. IEEE performs final layout in-house to distribute figures and tables within the text.

PR - 312

Center for Electromechanics
The University of Texas at Austin
PRC, Mail Code R7000
Austin, TX 78712
(512) 471-4496

May 3, 2002

Light-weight Containment for High Energy Rotating Machines

Joseph L. STRUBHAR, Richard C. THOMPSON, Tony T. PAK,
Joseph J. ZIERER, Joseph H. BENO, and Richard J. HAYES

***Abstract*-- The University of Texas Center for Electromechanics (UT-CEM), as a member of the Defense Advanced Research Projects Agency (DARPA) Flywheel Safety and Containment program, has developed a lightweight containment system for high-speed, composite rotors. The containment device, consisting of a rotatable, composite structure has been demonstrated to contain the high-energy release from a rotor burst event and is applicable to composite rotors for pulsed power applications. UT-CEM recently conducted a burst spin test of a composite flywheel inside this composite containment device at Test Devices Incorporated (TDI) of Hudson MA. The most important aspect of this design is that the free-floating containment structure dissipates the major loads (radial, torque, and axial) encountered during the burst event, greatly reducing the loads that pass through the stator structure to its attachments. The design results in significant system-level weight savings for the entire rotating machine when compared to a system with an all-metallic containment. Of equal interest to the containment design, the experimental design and instrumentation was very challenging and resulted in significant lessons learned. This paper describes the containment system design, rotor burst test setup, instrumentation for measuring loads induced by the burst event, and a detailed explanation of the successful containment test results and conclusions.**

I. Introduction

The energy storage potential of a flywheel is proportional to its mass moment of inertia and the square of the rotational speed. For a specific configuration, speed is limited by the material strength-to-density ratio. In terms of performance, high strength composite materials are currently the preferred flywheel material [1]. Furthermore, while metal wheels may provide a lower cost, albeit heavier, alternative for small stationary applications, composite flywheels will be required to meet the weight requirements for vehicular and aerospace applications. It is also apparent that to maximize energy storage in composite flywheels, they will operate at high rotational speeds.

Manuscript received January 14, 2002. A portion of this research was carried out under the DARPA Containment Projects sponsored by the Southern Coalition for Advanced Transportation under contract number MDA972-94-2-0003. Authors are affiliated with The University of Texas at Austin Center for Electromechanics, Austin, Texas 78758, (512) 471-4496, fax (512) 471-0781.

Due to a long history of operating experience, a great deal is known about the failure modes of metallic flywheels and the public has grown accustomed to using them in many everyday applications. This includes their use as power smoothing devices in manual transmission passenger cars, where the flywheel resides in close proximity to both the driver and passenger. Because metallic wheel failure mechanisms are well characterized, there is little reason for concern if standard engineering practices are applied. In contrast, little data has been published about failure modes and containment of composite flywheels. However, it is known that (1) composite rotor failure modes are very different from the behavior of metallic wheels and (2) catastrophic burst failures with very rapid energy release during overspeed of composite flywheel rotors have been demonstrated during failure testing [2,3,4,5]. Based on the potential for catastrophic failure and the lack of long term operating experience with composite flywheels, it is prudent to incorporate containment structures to mitigate the effects of a failure in near-term vehicular Flywheel Energy Storage Systems (FESS). (While this is the approach taken by the U.S. FESS industry, it should be noted that low stress composite vehicular flywheels have been successfully operated without dedicated containment systems in Germany for many years, with no serious accidents reported [6,7]).

II. Design Overview

Fig. 1 shows the containment system and burst test device, referred to as the full scale containment (FSC), in section view. Two torque beams, shown as part number 1 in the figure, measure the amount of torque transmitted to the housing during the burst event. Each torque beam is fitted with two strain gauges that transmit the beam's deflection to the data acquisition system for future translation into torque measurements. Part #2 in Fig. 1, the adapter plate, serves as an interface between the containment experiment and the spin pit lid. The experiment is intended to replicate, as closely as possible, the dimensions and operating conditions that similar devices will see in future applications. To that end, parts 10 and 15 of Fig. 1 simulate vacuum housing components and serve to position the composite liner.

Parts 4, 6, 7, 8, 13, and 14 comprise the composite liner. L1 and L2, parts 7 and 8, provide the majority of the hoop strength of the liner having 90% and 80% (respectively) of their fibers wound in the hoop direction. These parts were designed to absorb the high radial loads resulting from the initial impact of flywheel debris plus the spin loads associated with the debris rotation. A portion of L1 consists of alternating layers, at a ratio of 1:1, of hoop windings and axial hand lay-ups. This portion is threaded in the finished part and contributes the majority of the axial strength of the liner. The G-10 end plates at either end of the liner axis are designed to absorb the high axial loads that had previously been observed after flywheel bursts. The axial loads are primarily caused by flywheel debris that is redirected axially after impacting the containment rings (parts 6, 7, 8, and 14 in Fig.1) As composite material from the failed ring strikes the end plates, the material drives the end plates outward axially against the dramatic taper of the upper and lower wedges. This displacement consumes some of the energy of the material and increases the volume of empty space necessary for flywheel rotor debris immediately surrounding the flywheel. During the burst event, rotating flywheel debris transmits angular momentum to the containment system. Additionally, as the debris fills the space between the flywheel and the containment, a braking effect takes place, resulting in transmission of angular momentum from the portion of the rotor that did not experience burst failure to the containment system. Consequently the flywheel, its debris, and the containment rotatable liner reach the same angular velocity and then subsequently spin down. As will be described later, the total time between burst and ultimate spin down was approximately 2 min, resulting in greatly reduced peak loads compared to other containment designs that dissipate the flywheel energy much quicker. The flywheel loses energy in overcoming the inertia of the stationary liner. The liner is designed to rotate freely minimizing torque transmitted to the housing. By reducing the mechanical demand on the housing it can be designed at a reduced weight.

The flywheel used for the test was modified to burst the outer banding at about 40,000 rpm. This was accomplished using an outer flywheel banding of carbon fiber with 40% of the tensile strength of the fibers used in the rest of the flywheel rim.

III. Design Methodology

Metal Support Structure – The FSC was designed based on loads seen in past containment experiments performed by UT-CEM. Using data from these tests engineers predicted mechanical demands on the containment system to be as high as 100,000 lb axial load, 400,000 ft-lb torque load, and 500,000 lb side load.

A major goal of the rotatable composite containment design is to reduce the peak loads ultimately transmitted to the aluminum vacuum housing and the flywheel mounting system.

*Composite Liner –T*he composite liner was designed around the following criteria: 0.100 in. gap between flywheel and liner, 32 ksi transient radial pressure, 12 ksi centrifugal radial pressure, 32 ksi transient axial pressure.

The flywheel is completely entrapped by the composite liner making it extremely difficult to inspect or remove after assembly, so disassembly features were designed into the composite liner to be tested. This was accomplished by adding a male buttress thread into the outer diameter of the lower wedge. A matching female thread was machined on the inner diameter of L1. As the female thread only covered half the axial length of L1, there was a 3/4 in. thread relief approximately 7 in. from the bottom face of L1. (Note: this thread relief will be important in the discussion of results later) This arrangement allows the containment liner to be opened for access to the flywheel by unscrewing and removing the lower wedge and endplate. It was important to have the threads present in the containment test as they would be in the fielded systems because it was uncertain how well they would perform under burst loading.

Critical Flywheel Parameters – Table 1 presents critical design parameters for the flywheel to be tested.

IV. Test Set-Up

The FSC was outfitted with a variety of instrumentation to establish the loads transmitted to the containment housing. The following discussion addresses areas of specific interest to the design team.

Torque – Torque measurement hardware includes two torque beams that function much like load cells. Strain gauges were attached on opposing faces of the torque beams such that any deflection of the beam would generate two strain readings of equal magnitude and opposite sign, i.e. compression and tension. Knowing the radial location of the torque pins, which react against the beams, facilitates the calculation of torque values from strain readings (Fig. 2).

Axial and Hoop Loads in Metal Housing – Paired axial and hoop strain gauges were used to measure loads in the aluminum housing at four locations spaced 90° apart on the housing midplane. This gives a total of four axial and four hoop strain gauges surrounding the full 360° of the housing (Fig. 3)

Housing Displacement – Designers wanted to measure the axial and radial displacement of the housing during the burst event. To see the maximum displacement it was necessary to look at the bottom end plate: the housing was viewed as a cantilevered beam with the unsupported end having the largest deflection. Bentley Nevada displacement probes with axial and radial orientations were chosen for

the measurements. Two sensor mounting blocks with one axial and one radial probe each were used with an intervening 90° arc between them (Fig.4).

Flywheel Speed and Performance – The experiment involved three methods for monitoring flywheel speed and performance. The spindle displacement probe measures the amount the spindle strays from the experiment's centerline in thousandths of an inch or "mils." This sensor is the first to warn of an imbalance due to any cause, including separation of flywheel composite bands, contact with the containment liner, or loss of flywheel material. During the data reduction phase, burst and spin down events can be linked to the dramatic jump at burst in the spindle displacement probe's output signal to establish the sequence of events in time.

Next on the list of flywheel monitors is the analog speed sensor. This sensor gives a voltage output directly proportional to the number of rotations per minute (rpm). It serves as a backup for the air turbine speed pickup.

The air turbine speed pickup, also referred to as the keyphaser, gives a single square pulse for each revolution of the air turbine and, therefore, the flywheel. RPM is measured indirectly by counting the number of pulses per unit time.

Composite Liner RPM – The strategy for absorbing energy from the flywheel after the burst requires that the composite liner rotate. To quantify the amount of energy donated to the liner it is essential to know the number and speed of liner rotations. To accomplish this, for the first time in a containment test, a Hall-effect sensor mounted in the bottom plate was employed (Fig.4). This device requires a magnetic target to trigger its output. Four nickel-plated magnets were recessed and epoxied at 90° intervals into the bottom face of the containment liner to trigger four square pulses per revolution of the liner.

Temperature – Temperature was recorded during the experiment using a thermocouple affixed to the stainless steel bottom plate. The particular location on the bottom plate (Fig. 4) was chosen because it is directly under the face of the composite liner. This would be where the majority of energy would be ultimately dissipated, through friction between the liner and the bottom plate as the liner rotates.

Housing Internal Pressure – In an actual application, the housing surrounding the composite liner would serve as a vacuum vessel. Sealed from atmosphere, this vessel would have to withstand any pressures generated within it during a burst. To establish what these pressures might be, a dynamic pressure transducer was installed in the bottom plate (Fig. 4).

Miscellaneous Instrumentation – Other instrumentation includes the TDI reference signal and the in pit microphone. The reference signal was recorded on one set of data tapes to have a signal of known frequency and amplitude to compare with instrumentation data and serve as a calibration baseline during the data reduction process. The in pit microphone was intended to record noise levels outside the containment device after the burst event and loss of vacuum in the spin pit.

V. Test Results

The burst event occurred at 39,500 rpm. Spin down required 120 s. Post-test inspection showed that the radial and axial burst event energies were successfully contained. The following more detailed observations were made as a result of the test:

Contact with Sensor Mounting Blocks After lifting the experiment out of the spin pit, the sensor mount was disassembled. The clearance between the sensor blocks and the bottom plate, approximately 0.25in., was gone and the gussets were in contact with the sensor blocks. Since there was no obvious deformation of the sensor mount, the loss of clearance between the bottom plate and the sensor blocks had to have been the result of elongation of the containment housing.

Upper Flange Deformation – The upper housing flange, having only six 0.75 in. bolts on a 30.25 in. bolt circle, had undergone plastic deformation. Later measurements would show the total axial elongation to range from 0.150 to 0.260 in. The lower strain values in the range corresponded to the sides of the containment that contacted the two sensor mounting blocks. The lower flange on the containment housing had sixteen 0.5 in. bolts on a 27.5 in. bolt circle and showed no signs of deformation. Cracks in the housing accompanied the bolts in those areas with the largest strain values. This deformation also destroyed the Bentley Nevada Probes.

Flywheel and Liner Condition – The remainder of the flywheel remained attached to the spindle during spin down. The following observations were made by viewing the flywheel and composite liner through the top of the containment housing: presence of a large gouge in the upper face of the flywheel; a blue discoloration of the titanium flywheel hub; an upward displacement of the flywheel until upper flywheel face contacted the upper bushing; a "step" on upper surface of the composite liner; and an inward rather than outward movement of the upper G-10 end plate.

Debris Packing – A small amount of fine debris, ranging in size from human hair to dust, escaped from the gaps between the upper containment housing flange and the adapter plate. The oil from the failed turbine joint fouled the debris. The top G-10 end plate had little more than a dusting of debris. The majority of the flywheel material packed into the spaces below the flywheel. Debris was packed so tightly between the bottom bushing and the bottom G-10 end plate that the liner could not be separated from the bottom plate/bottom bushing assembly. The bottom-bushing flange had to be cut off and a hoist used to pull the liner free. Engineers also observed asymmetric debris packing, that is, one quadrant of the liner being more

densely packed than other areas. Debris in the lower spaces ranged in size from dust and down-like material up to large segments of flywheel lamination material. Flywheel banding debris also managed to intrude into the spaces behind the two G-10 end plates. Also among the debris were some small pieces of the magnets used as targets for the hall probe tachometer. No magnets remained intact inside their recesses on the bottom face of the liner.

G-10 End Plates – Measurements of the final positions of the two G-10 end plates showed that they did not move outward, i.e. away from the flywheel, according to design but actually moved inward slightly. Table 2 summarizes the measurements of the endplates and their positions. The measurements of the net displacement of the lower wedge ranged from 0.030 to 0.300 in. Similarly, the net displacement of the upper wedge ranged from 0.39 to 0.52 in.

Failure of Composite Components – Observation of the step in the upper surface of the composite liner led to the initial conclusion that the bond line between the upper wedge and L1 had failed under axial load. Later inspection proved (by measuring the diameter of the raised circular step) that the failure actually occurred within the threaded section of L1. To facilitate inspection in the lab at UT-CEM, the upper and lower wedges, L1 and L2 were split axially and it was clear that the interlaminar failure of L1 initiated at the thread relief. A large segment of the outer flywheel ring was embedded in the volume created by the thread relief and the axial displacement of the inner laminations of L1. Sectioning the composite liner also showed the failure of the threads in the lower wedge. Both external "male" threads on the lower wedge and internal "female" threads on the inner diameter of L1 failed during the test.

Instrumentation – Not only were the Bentley Nevada probes were destroyed during the test, but the accelerometers mounted in tandem with them saturated with the impact so that data from them was meaningless. Readings from the tachometer were inconsistent and, given that no magnet targets survived the test, information from the tachometer is considered unreliable. The pressure transducer also gave no indication of a pressure rise within the housing. A summary of results is offered in Table 1.

VI. Discussion of Results

Thread Relief and Threads – Various theories exist as to the nature of the failure emanating from the thread relief. One theory suggests that the large segment of intact flywheel banding material created a wedging effect, much like a log splitter, that drove the upper and lower sections of L1 apart. The banding material accessed the thread relief through the split between the upper and lower wedges. Another theory claims that the stress concentrations at the thread relief sufficiently weakened L1 that it was unable to withstand the shear from the axial loads on the G-10 endplates. In this second theory, the axial loads opened the void at the thread relief and created a pocket for the banding material to recede into, thus sheltering the debris segment from the destructive forces of the spinning flywheel

Flange Design in Aluminum Housing – The upper flange on the aluminum housing failed due to having too few bolts on too large a bolt circle. The bolt pattern was used to match an existing bolt circle in the adapter plate. Insufficient material was provided for the housing to withstand the bending moment on the flange created by axial loads on the housing.

FEA analysis using COSMOSWorks indicates that modifying the top flange to have the same bolt circle as the bottom housing flange and increasing the fillet radius to 0.375 from 0.25 reduces stresses in the cracked regions of the housing by 60%.

Improvement in Instrumentation – The Hall-effect tachometer showed that there was some rotation of the composite liner, but the number and frequency of rotations was unclear. The Hall–effect probe showed erratic values from 6,000 to 57,000 rpm.

Torque measurements also produced unexpected results in that both torque beams were seldom loaded simultaneously. Since the beams were positioned closely to their respective torque pins during the assembly of the experiment, one would expect to see simultaneous loading; however, the data show that there was significant delay between peaks on the torque beams. In fact, for the first few milliseconds of the burst event, the outputs from torque beams A and B are 180^{o} out of phase. This is consistent with loading and unloading the torque beams through radial displacements of the housing due to mass loading.

There is additional evidence of radial translation of the entire experiment in the data from the Bentley Nevada probes. Average gap between the radial probes and the stainless steel bottom plate was 0.045 in. at the start of the test. If one treats the containment housing as a cantilevered beam, the force required to cause this displacement can be found to be approximately 85 ksi using Timoshenko [8]. This is nearly twice the ultimate strength, 45 ksi, of the 6061-T6 aluminum. While it is known that the material did fail at the upper flange, there were no strain readings in the housing indicating the level of stress that would accompany bending loads as large as that calculated above. In addition, at the same point in time that the large displacement occurred, three of four strain gauges were in tension. Bending stress would create compressive as well as tensile readings in the strain gauges. These three clues: the phased loading of the torque beams; the impossible calculated load on the bottom end plate; and the tensile axial strains; strongly suggest that the observed displacement of 0.045 in. is only possible if the entire experiment translates on its mounts. With such lateral motion it is possible to load the torque beams and cause a torque reading without actually generating a true torque on

the housing. Torque beams show a maximum force of 51,000 lbf (giving a torque of 63,000 ft-lb), but this load could be from any combination of torque and radial load. The additional possibility exists that the containment experienced larger radial loads, but they were perpendicular to the loading direction that would be registered by the torque beams, i.e. along the longitudinal axes of the torque beams.

Load Reductions – What is certain is that torque values never exceeded 63,000 ft-lb, meaning that torque loads on the containment system were reduced by an order of magnitude over the past 400,000 ft-lb value. In addition, it is most likely that no side load exceeded 51,000l b_f , again a reduction of an order of magnitude over results seen in past tests.

VII. Recommendations

Threads and Thread Relief – Future designs will require the elimination or relocation of the thread relief. The "log splitting" theory demands that future designs move the thread relief away from the plane of rotation of any flywheel debris. The other theory that axial loads from the G-10 end plates ripped L1 apart suggests that the thread relief be removed entirely. In either case, it would be advantageous to shield the thread relief if it is retained in future designs.

Flange in Aluminum Housing – The housing will require modification in accordance with observation and the FEA modeling described. This will entail the reduction of the upper flange bolt circle diameter, the increase in the number of bolts in the upper flange, and the increase of the fillet radius joining the flange to the housing wall.

Instrumentation – The experiment requires a more stable attachment to the spin pit lid. Eliminating relative motion between the pit lid and experiment would improve torque readings and allow closer placement of sensors if the need arises.

The Hall Effect probe tachometer would have provided useful information had the target magnets survived. Future containment experiments should identify a better method for shielding and retaining the magnets.

VIII. Conclusions

An understanding of flywheel failures and their containment is critical to gaining acceptance for flywheels in the vehicular market. This experiment achieved a significant milestone by demonstrating the safe containment of a flywheel failure at full speed.

While the experiment was successful and proved the viablity of a rotating composite liner, it also identified a number of areas where the design and instrumentation could be improved. Based on these results, UT-CEM has designed an updated version of this system which incorporates the critical features identified in the Recommendations above. This system will be tested in 2002 and results will be reported in future technical papers.

Acknowledgment

The authors would like to acknowledge the support of the organizations who provided funding for this project: Southern Coalition for Advanced Transportation (SCAT); Defense Advanced Research Projects Agency (DARPA); and the Houston Metropolitan Transit Authority (HMTA). Also appreciated is the technical expertise of individuals at UT-CEM: Mr. Robert Arndt, who was responsible for fabrication of the containment and test conduction; Ms. Lori Moore and Ms. Vicki Heydron, who were responsible for preparing this manuscript; and Mr. Roy Pena and Mr. Rex Jackson, who contributed graphics support.

References

[1] Stull, S. and Post, R.F., "A New Look at an Old Idea" Science and Technology Review, pp.12-19, April 1996.

[2] "Spin Test Tragedy" Performance Materials, pp1-3, Volume 11, Number 4, Nov. 20, 1995.

[3] Rabenhorst, D.W. and Small, T.R., "Spin Test of the University of California Lawrence Livermore Composite Flywheel at the Applied Physics Laboratory of the Johns Hopkins University", UCRL 13910, pp 1-14, July 18, 1978.

[4] Coppa, A.P., "Composite Flywheel Containment Housing Design and Testing", Section V, pp 1-12, UCRL 15448-Vol.2, DE85 001042.

[5] Kass, M.D. et al,"Evaluation of Demo 1C Composite Flywheel Rotor Burst Test and Containment Design" pp. 14-20, Oak Ridge National Laboratory TM-1315, March, 1996.

[6] G. Reiner et. al., "Experiences with the magnetodynamic (flywheel) storage system (MDS) in diesel electric and trolley busses in public transport service," Presentation at Flywheel Energy Storage Technology Workshop, Oak Ridge Tenn., November 1993.

[7] Magnet-Motor Gmbh, Starnberg, Germany, <http://www.magnet-motor.de>, accessed January 14, 2002

[8] J.M. Gere, S.P. Timoshenko, *Mechanics of Materials*. Boston, MA: PWS, 1990, pp. 260, 772.

TABLE 1
CRITICAL FLYWHEEL PARAMETERS

Composite flywheel outer diameter (at rest – large end)	17.894 in.
Composite flywheel outer diameter (at rest – small end)	17.644 in.
Composite flywheel inner diameter (at rest)	6 in.
Outer composite ring radial thickness	0.5 in.
Axial length of flywheel	5 in
Flywheel radial taper (per side)	1.47°
Flywheel weight including titanium hub	95 lb
Energy stored at 38,500 rpm	7 MJ
Energy stored in outer ring at 38,500 rpm	1.4 MJ
Weight of outer ring	8 lb

TABLE 2
RESULTS SUMMARY

Component	Observation
Debris	Dense packing of debris in lower regions of containment; some magnet pieces from tachometer targets found; large intact segment of flywheel banding found embedded in thread relief
G-10 end plates	Upper G-10 end plate had a net OUTWARD movement of 0.123 in. and moved inward relative to the upper wedge 0.46 in. Experienced wear to its inner surface of 0.060 in. (at the point of greatest wear) Lower G-10 end plate had a net INWARD movement of 0.156 in. and moved inward relative to the lower wedge 0.165 in.
Composite liner	Interlaminar failure in L1 initiated at thread relief; both male and female threads failed
Aluminum housing	Total axial elongation of housing from 0.150 to 0.260 in.
Torque beam A	63,000 ft-lb; 5 ms after burst
Torque beam B	43,000 ft-lb; 25 ms after burst
Max hoop stress (compression)	-45 ksi; 20 s before tensile hoop reading (all 4 hoop strain gauges in compression)
Max hoop stress (tension)	27 ksi; 2 strain gauges in tension, 2 in compression
Max axial stress (compression)	-18 ksi; 40 s before tensile axial reading (1 strain gauge in compression, 3 in tension)
Max axial stress (tension)	22ksi; all strain gauges in tension
Tachometer (flywheel)	Spin down time 120 s
Tachometer (liner)	Inconclusive
Thermocouple	105° F from 70° F in 276 s
In-pit microphone	Nothing recorded

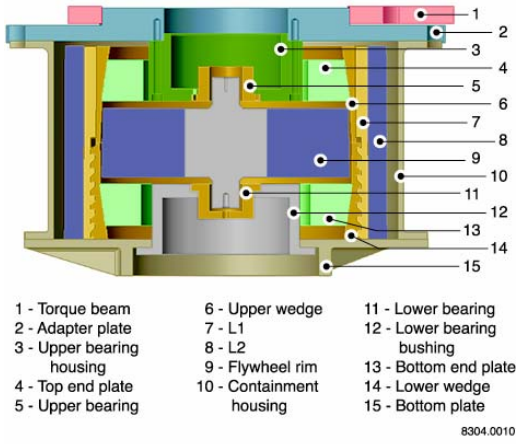

Figure 1. Assembly cutaway

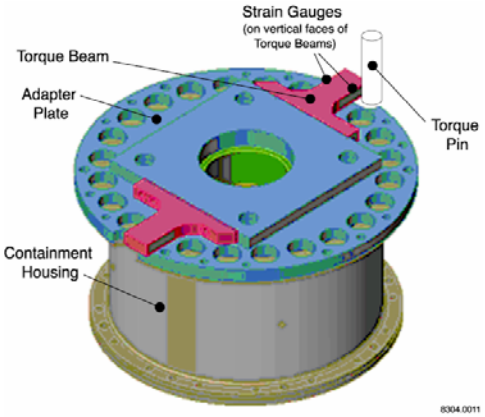

Figure 2. Torque measurement

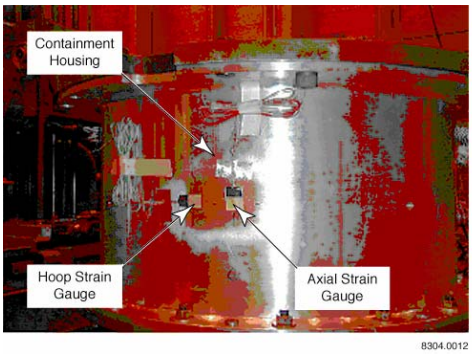

Figure 3. Axial and hoop strain gauge locations

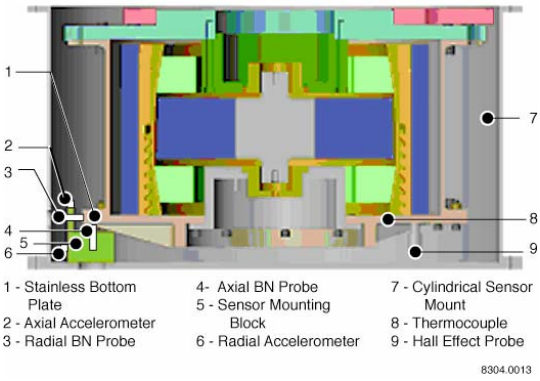

Figure 4. Sensor locations for spin test

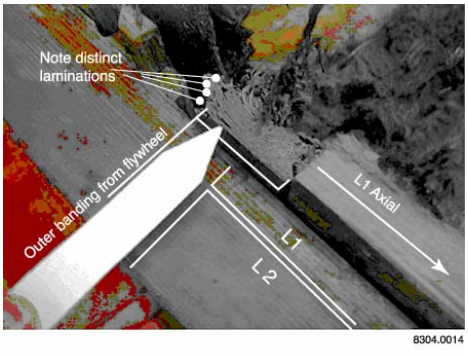

Figure 5. Composite component failure